ACS OMEGA

Article

Cite This: ACS Omega 2019, 4, 3732−3738

http://pubs.acs.org/journal/acsodf

Boron−Carbon−Nitride Sheet as a Novel Surface for Biological Applications: Insights from Density Functional Theory

Showkat Hassan Mir, Vivek Kumar Yadav, and Jayant Kumar Singh*

Department of Chemical Engineering, IIT Kanpur, Kanpur208016, India

Supporting Information

ABSTRACT: Understanding the interaction between nanoscale materials and nucleobases is essential for their use in nanobiotechnology and nanomedicine. Our ab initio calculations indicate that the interaction of nucleobases [adenine (A), cytosine (C), guanine (G), thymine (T), and uracil (U)] with boron−carbon−nitride (BCN) is mainly governed by van der Waals interactions. The adsorption energies, ranging from −0.560 to −0.879 eV, decrease in the order of G > A > T > C > U, which can be attributed to $\pi-\pi$ interactions and different side groups of the nucleobases. We found that anions (N and O atoms) of nucleobases prefer to stay on top of cation (B) of the substrate. The results also showed that BCN exhibits superior binding strength than graphene and boron−nitride-based materials. We also found that upon adsorption, the fundamental properties of BCN and nucleobases remains unaltered, which suggests that BCN is a promising template for self-assembly of nucleobases.

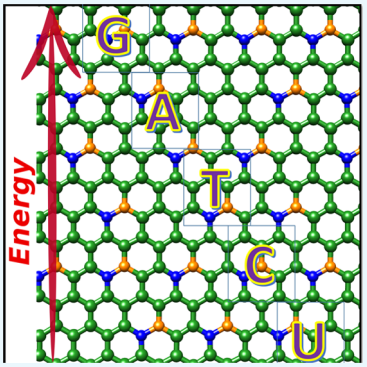

INTRODUCTION

The adsorption of purine [adenine (A), guanine (G)] and pyrimidine [cytosine (C), thymine (T), uracil (U)] nucleobases onto the surfaces of inorganic solids has long been considered a process relevant to the origin of life.[1] The interaction of nucleobases with inert surfaces has garnered significant attention due to its importance for self-organization and molecular recognition process.[2] Adsorption of nucleobases on nanomaterials is beneficial for delivering therapeutic nucleic acids,[3,4] developing smart stimuli-responsive materials,[5,6] and designing biosensors.[7−9] Two-dimensional (2D) materials due to their large specific surface area have emerged as a unique platform for interfacing with nucleobases. Developments in this field were stimulated by the discovery of graphene.[10] Several nanomaterials, such as quantum dots,[11,12] carbon nanotubes,[13] and graphene oxide (GO),[14−17] have been used to sense DNA nucleobases (A, C, G, T) using fluorescent[18] and calorimetric[19] assessment. For instance, 2D sheets of graphene,[20,21] graphene oxide (GO), and hexagonal boron nitride (hBN)[22,23] have been reported to sense gas molecules and biomolecules.[24] The interaction between DNA molecules and GO was extensively, studied which has lead to the exploration of other 2D materials.[14−17]

Previous theoretical calculations performed within the framework of local density approximations (LDAs) have shown that binding energy of nucleobases on graphene follows the order as G > A ≈ T ≈ C.[21] Calculations performed with density functional theory (DFT) methods, including van der Waals (vdW) interactions[25,26] as well as using a more accurate second order Møller−Plesset perturbation theory (MP2)[21] demonstrated that the binding strength of nucleobases with graphene exhibits the hierarchy as G > A > T > C. These findings are consistent with the single solute adsorption isotherm study at the graphite−water interface.[1] Interaction of nucleobases has also been studied intensively on hBN sheet,[2,13,27] which was successfully fabricated through a chemical solution-derived[28] method and microchemical cleavage method.[29]

The hBN shows a honeycomb lattice structure similar to that of graphene; however, its electronic properties are entirely different from that of graphene. Graphene is a semimetal with 0 eV band gap[30] and having a nonpolar nature of C−C bond, whereas hBN is an insulator (band gap ≈6 eV) with polar B−N bond due to charge transfer from B to N atom owing to their different electronegativities.[31,32] Using LDA scheme, Lin et al. studied the adsorption of nucleobases on hBN and concluded that nucleobases bind to the hBN through polar electrostatic interaction, which manifests that nucleobase−BN interaction is somewhat different from the $\pi-\pi$ interaction between nonpolar graphene and nucleobases.[27] The hierarchy of the adsorption energy of nucleobase molecules on hBN sheet found in this study was G > A > T > C > U.

Recently, transition-metal dichalcogenides also received considerable interest for the design of novel biosensors due to their large surface area and outstanding electronic and optical properties.[33,34] On the basis of photoluminescence measurements, Jin et al.[34] showed that Au-modified MoS_2 nanostructures allow rapid and sensitive detection of DNA. Loan et al.[35] designed graphene/MoS_2 heterostructures for label-free and selective detection of DNA by measuring the change in peak intensity of photoluminescence. Huang et al.[36]

Received: December 10, 2018
Accepted: February 12, 2019
Published: February 20, 2019

DOI: 10.1021/acsomega.8b03454
ACS Omega 2019, 4, 3732−3738

fabricated a microfluidic biosensor based on monolayer MoS_2 sheet for the ultrasensitive and visual detection of DNA.

Understanding the interaction of nucleobases with nanomaterials is important for the design of better sensors with high selectivity. In this article, we report the adsorption of nucleobases on the hybrid structure of graphene and hBN. The ternary boron−carbon−nitride (BCN) alloy is a graphenelike nanostructure wherein some carbon atoms are substituted by boron and nitrogen. These new hybrid structures constitute an important material as their band gap can be tailored by varying the atomic composition and atomic arrangement.[37,38] Hybrid structures of graphene doped with nanodots of BN have been synthesized experimentally.[39,40] The effect of geometry and position of nanodots on the structural, electronic, and magnetic properties has been studied extensive using density functional theory.[38,41,42] Recently, Chhetri et al. demonstrated that BCN sheet show superior performance as a metal-free electrocatalyst for hydrogen evolution reaction.[43]

Understanding the interaction between solid surfaces and biologically active molecules, such as nucleic acid or proteins, is essential for the preparation of biocompatible materials and biosensors.[44] In addition, the self-assembly of DNA bases on the inert surfaces has been hypothesized to play a crucial role in the emergence of life under prebiotic conditions. Our findings showed that BCN is a promising template for the self-assembly of nucleobases.[27] Therefore, in this work, we report the binding affinity of nucleobases with the BCN sheet. The paper is organized as follows: in Computational Methodology, we provide details of the methods used in this work. In Results and Discussion, we discuss the structural and thermodynamic stability of BCN sheet by calculating its cohesive and formation energy. Thereafter, we analyze the binding strength of nucleobases on BCN sheet. To give further insight on the binding strength of nucleobases with BCN, the electronic band structure of pristine and nucleobase-adsorbed BCN sheets was also examined, followed by work function calculation. We concluded the paper by giving a detailed summary of the main results obtained and the future scope of boron−carbon−nitride hybrid structures.

RESULTS AND DISCUSSION

Structural and Thermodynamic Properties. The thermodynamic stability of the BCN sheet was assessed by calculating its formation and cohesive energies. The formation energy (E_f) and cohesive energy (E_{coh}) were calculated using eqs 1 and 2. It is important to note that with this approach, the formation energy of pristine graphene and hBN sheet is equal to zero, which provides us a reference value to compare the formation energy of BCN sheet with these 2D structures. The equations used to calculate E_{coh} and E_f of BCN are given below.

$$E_f = [E_{BCN} - (n_{CC}\mu_{CC} + n_{BN}\mu_{BN})]/N \quad (1)$$

$$E_{coh} = [E_{BCN} - \sum_i N_i E_i]/N \ (i = C, B, N) \quad (2)$$

where, in eq 1, n_{CC} (=28) and n_{BN} (=8) denote the CC and BN pairs in the BCN sheet and μ_{CC} and μ_{BN} corresponds to the chemical potential of C−C and B−N, respectively. The chemical potentials C−C and B−N were obtained directly from the infinite sheet energies of graphene and hBN. On the other hand, in eq 2, E_i represents the gas-phase atomic energies of C, B, and N. E_{BCN} represents the total energy of BCN. The formation and cohesive energies calculated for BCN sheet are 0.21 and −7.4 eV, respectively. These results indicate that BCN is thermodynamically stable. To compare the thermodynamic stability of the BCN with graphene and hBN, we also calculated the formation and cohesive energies for these systems. Our results indicate that the stability of BCN lies midway between that of graphene and hBN. The hierarchy in thermodynamic stability of the three systems follows the order as graphene > BCN > hBN, as can be seen in Figure 1. The

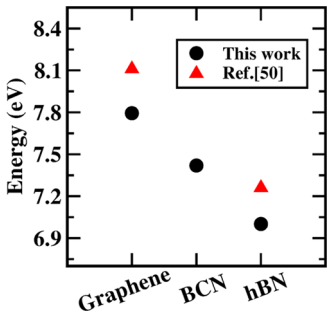

Figure 1. Cohesive energy of BCN sheet compared to that of graphene and hBN.

calculated cohesive energies show a similar trend, as predicted by Özçelik et al.[45] Our results predict comparatively smaller cohesive energies, which may be attributed to different functionals (projector augmented wave), as employed in ref 50 and ours Perdew−Burke−Ernzerhof (PBE). The chemical potential μ_{CC} and μ_{BN} obtained from graphene and BN sheet were −310.150 and −358.352 eV, respectively, which have been used in eq 1.

The optimized structure of BCN is shown in Figure SI2. Its optimized dimensions in the plane were 14.760 × 14.760 Å^2. The calculated C−C, C−N, C−B, and B−N bond lengths were 1.423, 1.376, 1.476, and 1.455 Å. Optimized structures of nucleobases in the gas phases are also shown in Figure SI2. From the figure, it can be seen that the nucleobase molecules are terminated at the cut bond to the sugar ring with a methyl group (CH_3) to create an electronic environment in the purine and pyrimidine bases more closely resembling their situation in extended chains rather than that of just individual isolated nucleobases by themselves.[21] This also has an advantage of creating a certain level of steric hindrance during the interaction with the substrate.

Binding Energy. We start out this section by describing the optimized structures of A, C, G, T, and U adsorbed on BCN using PBE and PBE + vdW schemes. Since, in the previous theoretical studies, it is reported that the nucleobases prefer to orient parallel on graphene and hBN with AB-stacking owing to $\pi-\pi$ interaction,[27,46,47] in this work, we calculated the binding energy of nucleobases on BCN sheet using AB-type stacking. The optimized structures of nucleobases adsorbed on BCN sheet using PBE + vdW are presented in Figure 2. From the optimized structures of nucleobases on BCN with AB-stacking, we observed that the N atom of the nucleobase does not align itself over the nitrogen atom of BCN due to electrostatic repulsion. The AB-stacking structures of A, C, G, and T on BCN are very similar to that of graphene and hBN.[21,27] Table 1 presents the vertical distance between nucleobase molecules and BCN. We found that vertical distances calculated using the PBE functional are

DOI: 10.1021/acsomega.8b03454
ACS Omega 2019, 4, 3732−3738

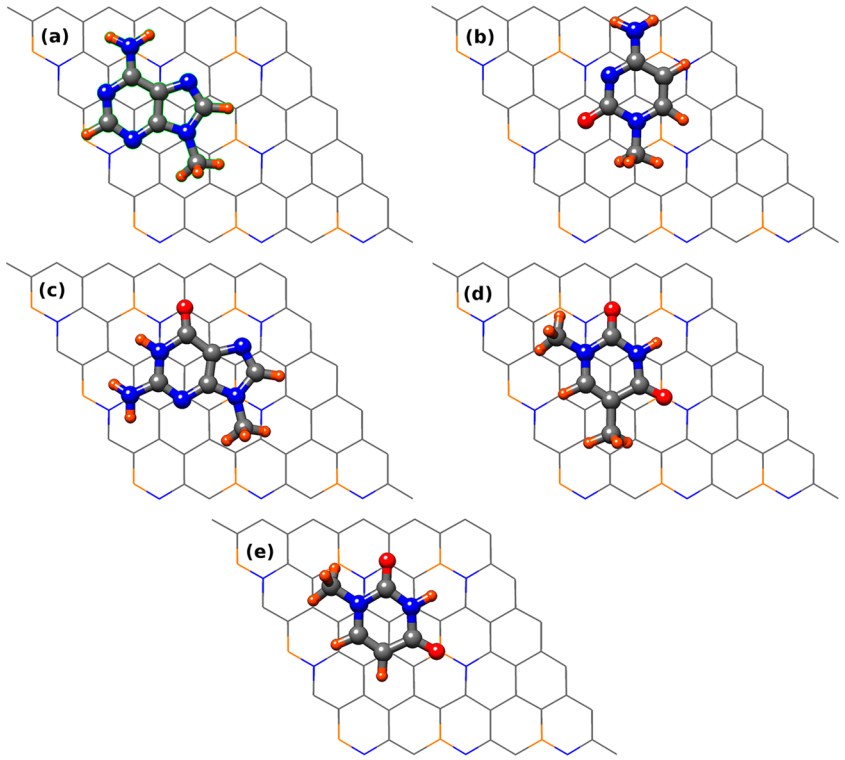

Figure 2. Optimized structures of (a−e) A-, C-, G-, T-, and U-adsorbed BCN. Gray, blue, red, orange, and orange-red balls represent carbon, nitrogen, oxygen, boron, and hydrogen atoms.

Table 1. Adsorption Energies (E_{ad}) of Nucleobases and Equilibrium Distances (Dist) between the Nucleobases and BCN[a]

	PBE + vdW		PBE	
nucleobase	E_{ad}	Dist	E_{ad}	Dist
BCN + A	−0.766	3.416	−0.076	3.852
BCN + C	−0.750	3.390	−0.078	3.902
BCN + G	−0.879	3.467	−0.089	3.789
BCN + T	−0.712	3.478	−0.073	3.952
BCN + U	−0.560	3.564	−0.060	4.093

[a]The energy is in eV, and distance, in Å.

comparatively larger than those of PBE + vdW. For instance, the PBE and PBE + vdW distances calculated for G on BCN were 3.789 and 3.467 Å, respectively. A similar behavior was observed for other nucleobases also. It is obvious that the calculated vertical distances are much larger than the typical covalent bond lengths, which indicates that there could not be any charge transfer between nucleobases and BCN. Moreover, it is worth mentioning that we did not find any buckling in the BCN or a tilt in the nucleobase molecules upon adsorption, which is a clear indication of $\pi-\pi$ interaction between nucleobases and BCN.

The binding energies of nucleobases calculated using PBE and PBE + vdW schemes are also given in Table 1. It is observed that PBE + vdW gives more binding than PBE due to dispersion correction in the former. The calculated binding energies obtained using PBE + vdW (PBE) are −0.766 (−0.076), −0.750 (−0.078), −0.879 (−0.089), −0.712 (−0.073), and −0.560 (−0.060) for A, C, G, T, and U, respectively. We found that purine bases show comparatively strong interaction to BCN than pyrimidine bases, which is due to the presence of two aromatic rings in them. The pyrimidine base (U) has least interaction as it contains only one ring and one side ($-CH_3$) chain. On the other hand, pyrimidine bases (C and T) exhibit intermediate interaction with the BCN because of the presence of two side ($-CH_3/-NH_2$ in C and $-CH_3/-CH_3$ in T) chains. The differences in the adsorption energies of nucleobases can also be explained on the basis of vdW forces, which are directly proportional to the mass and size of interacting species.[47] In addition, it is apparent that the calculated binding energies are comparatively much larger than those of gas molecules physisorbed (0.01−1 eV per molecule) on a solid surface but less than the chemisorbed energies (1−10 eV per molecule),[27] which also shows that nucleobases are adsorbed on the BCN. The order of binding strength of nucleobases on BCN sheet shows the trend as G > A > T > C > U for PBE + vdW (G > A > T > U > C for PBE). A similar order of binding energy for four nucleobases (A, C, G, and T) on graphene and hBN were observed in previous theoretical results.[21,27] It is also important to note that the calculated binding energies are comparatively larger than those calculated on hBN ribbon[47] (−0.433 to −0.624 eV), boron nitride nanotube (BNNT)[2] (−0.29 to −0.42 eV), hBN sheet (−0.50 to −0.69 eV),[27] and graphene[21,26] (−0.512 to −0.73 eV). The binding energy is also in good agreement with the results of Gowtham et al.[21] who employed MP2 perturbation theory to study the adsorption of nucleobases on graphene. The comparatively larger binding energy obtained in the present study is due to the Coulombic interactions that occur between nucleobases and substrates owing to the different electronegativities of boron and nitrogen besides $\pi-\pi$ interactions. Also, as DFT calculations are performed in gas phase and the interaction energies may change in a more realistic environment such as water, it is essential to compare the theoretical

DOI: 10.1021/acsomega.8b03454
ACS Omega 2019, 4, 3732−3738

results with experimental data. It is worth mentioning that our DFT results showed the same trend of interaction of nucleobases with the BCN as experimental studies have observed on graphene[48] and crystalline graphite[1] in water. In addition, from Table 1, it is observed that binding energies calculated using PBE are smaller as compared to PBE + vdW of about 1 order of magnitude. This shows that the physisorption of nucleobases on BCN is mainly governed by vdW interactions. This also demonstrates the necessity of including vdW forces for studying nucleobase interactions with a surface.

Electronic Structure. Band structure calculations of nucleobase-adsorbed BCN are important to analyze the binding mechanism of nucleobases with the sheet. Table 2 shows the Fermi energy, highest occupied molecular orbital (HOMO), lowest unoccupied molecular orbital (LUMO) energy, and band gap of bare and nucleobase-adsorbed BCN. HOMO and LUMO energies and band gaps of nucleobases are also shown in Table SI1. The calculated HOMO−LUMO gaps are comparatively smaller for purine bases (2.766 eV for A and 2.499 eV for G) than pyrimidine bases (3.013, 3.364, and 3.664 eV for C, T, and U, respectively). The HOMO and LUMO energies lie in the range of −5.041 to −5.739 and −2.204 to −2.296 eV, respectively. This shows that electrons in the nucleobases are tightly bound to their respective molecules. The calculated band structures of bare and nucleobase-adsorbed BCN are presented in Figure 3. It is well known that graphene has a 0 eV band gap and exhibits a Dirac cone that arises as the conduction and valence bands touch each other at the symmetry *K*-point of the Brillouin zone (BZ). Furthermore, the experimentally measured band gap of hBN is ≈6 eV.[40] From the calculated band structure, it can be clearly seen that the BCN sheet shows a direct band gap that is also located at the Γ-point of the Brillouin zone. The calculated band gap of bare BCN is 0.659 eV, which is significantly less than that of hBN but greater than that of graphene. These results shows that the ternary alloy of boron, carbon, and nitrogen may have potential applications in electronics as it show a suitable direct band gap.

Table 2. Fermi Energy, HOMO and LUMO Energies, and Band Gap of Bare and Nucleobase-Adsorbed BCN Sheet[a]

system	E_{HOMO}	E_{LUMO}	E_{Fermi}	E_{gap}
BCN	−2.461	−1.801	−2.137	0.659
BCN + A	−2.253	−1.597	−1.930	0.656
BCN + C	−2.287	−1.628	−1.964	0.658
BCN + G	−2.195	−1.539	−1.872	0.656
BCN + T	−2.185	−1.528	−1.862	0.656
BCN + U	−2.248	−1.593	−1.925	0.655

[a]All energies are in eV.

In addition, it is important to mention that a band gap can be opened in graphene by introducing differently sized nanodomains in the graphene.[41] This indicates that by changing the composition of constituent elements in BCN, its band gap can be tailored for specific applications. Similarly, the band gap of hBN can be tuned by incorporating graphene nanodomains in it. In a recent study, Ba et al. experimentally synthesized these kinds of sheets wherein they cut down the band gap of hBN to ≈2 eV, which is about one-third of the band gap of pristine hBN.[40]

Now, considering the band structure of nucleobase-adsorbed BCN, we found that nucleobases have a negligibly small effect on the band gap of BCN, as can be seen from Table 2. The maximum change observed in the band gap of nucleobase-adsorbed BCN is 4 meV. These results clearly show that the fundamental properties (e.g., electronic structure and geometry) of BCN and nucleobases in the adsorbed state remain unaltered, which indicates that BCN is a potential candidate for the self-assembly of nucleobases and should be further explored for biological applications.

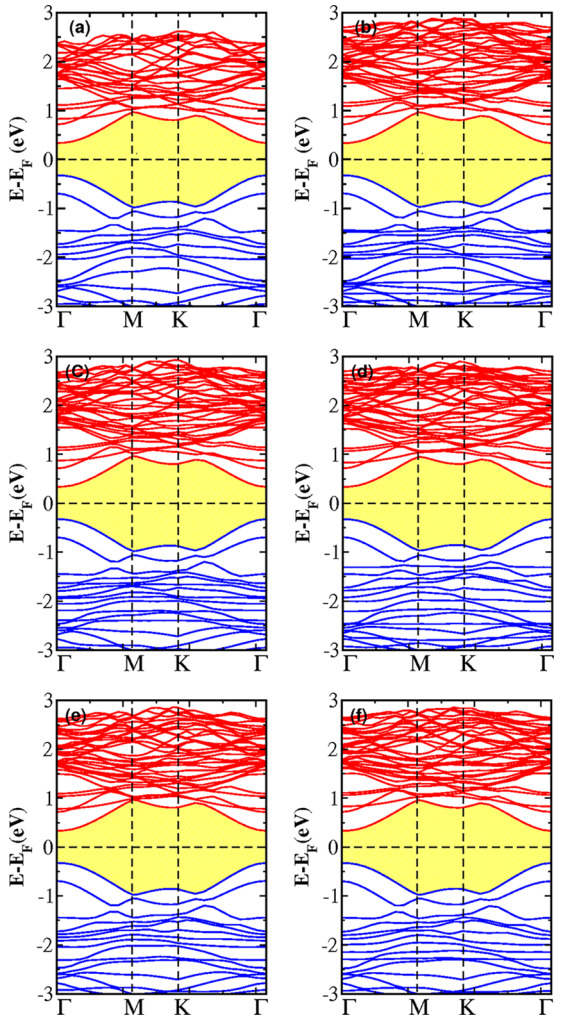

Figure 3. Band structure of (a) pristine, (b−f) A-, C-, G-,T-, and U-adsorbed BCN.

Work Function. To further understand the interaction of nucleobases with the BCN sheet, we calculated the work function (Φ) of bare and nucleobase-adsorbed BCN. Φ was calculated using eq 3 and is defined as the energy required for removing an electron from the Fermi level to the vacuum.

$$\Phi = E_{vac} - E_F \quad (3)$$

where E_{vac} represents the vacuum potential and E_F is the Fermi energy. The values of Φ calculated for bare and nucleobase-adsorbed BCN are 3.792 eV, 3.879 eV (A), 3.868 eV (C), 3.841 eV (G), 3.766 eV (T), and 3.812 eV (U). Plots of the work function are shown in Figure 4. The small dip in the work function corresponds to the position of nucleobases, whereas the larger dip is associated with the BCN sheet. We observe that upon adsorption, the work function of nucleobase-adsorbed BCN changes relative to the value of pristine BCN (3.792 eV) by 0.087, 0.076, 0.049, −0.026, and 0.020 eV for A,

DOI: 10.1021/acsomega.8b03454
ACS Omega 2019, 4, 3732−3738

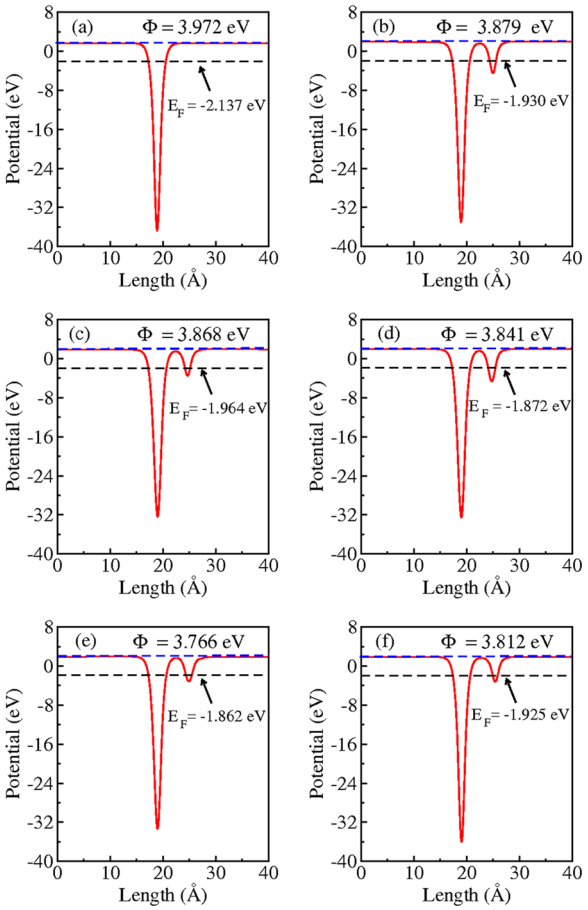

Figure 4. Work function plots of (a) pristine and (b–f) A-, C-, G-, T-, and U-adsorbed BCN. The dashed blue line represents the vacuum potential.

C, G, T, and U, respectively. These results show that work function of BCN changes distinctly upon adsorption of nucleobases, which shows the possibility of tuning the work function of substrate materials. The small changes in the work function also signify the physisorption of nucleobases on BCN. Also, due to the shift in the work function, there will be a small rearrangement in charge at the nucleobase–substrate interface. This rearrangement of charges produces an interfacial dipole moment, which can be related to the shift in work function $\Delta\Phi$. This work function shift, in turn, can be related with the change in the induced dipole moment (Δp) using a simple electrostatic relation[49] $\Delta\Phi = e\Delta p/\epsilon_0 A$, where A is the area of the cell used in the calculation. Employing this equation, we calculated Δp for adsorbed A, C, G, T, and U on BCN as 0.105, 0.091, 0.059, −0.031, and 0.024 e Å. It should be noted here that Δp represents the normal component of the induced dipole moment directed from nucelobases to the substrate ($\Delta p > 0$) and the substrate to nucleobases ($\Delta p < 0$). On this basis, it can be said that although the nucleobases are physisorbed on BCN, which is mainly caused by vdW interactions, an interfacial dipole is induced upon adsorption to produce a shift in the work function.

CONCLUSIONS

We performed ab initio calculations to study the thermodynamic stability and electronic structure of BCN ternary alloy and examined their interaction with nucleobases. Our calculations show that BCN is a thermodynamically stable material. Also, all five nucleobases were found to exhibit physical adsorption on the BCN, which is attributed to the $\pi-\pi$ interaction and their different molecular structures. Our results showed that the adsorption energy of nucleobases on BCN follows the order G > A > T > C > U. The adsorption energies calculated on BCN were found superior to graphene, hBN, and BNNT. Additionally, it is found that the interaction between nucleobases and BCN does not change their fundamental properties. On the other hand, nucleobases were found to significantly change the work function of BCN sheet due to charge rearrangement at the substrate–nucleobase interface. Thus, it can be concluded that BCN may act as a superior candidate for sensing applications and the self-assembly of nucleobases compared with graphene, hBN, and BNNT.

COMPUTATIONAL METHODOLOGY

DFT calculations were performed to study the adsorption energies and structural properties of bare and composite systems. The ground-state calculations were carried out using the Perdew–Burke–Ernzerhof (PBE) functional within generalized gradient approximation.[50] Ultrasoft pseudopotentials were generated using the Rappe–Rabe–Kaxiras–Joannopoulos method.[51] A kinetic energy cutoff of 40 Ry was employed for plane wave basis set and 400 Ry for charge density. The Brillouin zone (BZ) integration was done using a uniform Monkhorst–Pack[52] k-mesh of 3 × 3 × 1 point for relaxation calculations and 10 × 10 × 1 for electronic structure calculations. Both kinetic energy cutoff and k-mesh were found sufficient to satisfy convergence criteria (Figure SI1). We used a 6 × 6 × 1 unit cell consisting of 72 atoms in total, out of which 56 are carbon and 8 each are boron and nitrogen (making approx a ternary alloy consisting of $B_{0.1}C_{0.8}N_{0.1}$). To avoid the interaction between periodic images, a large vacuum of 20 Å was employed in a direction perpendicular to the sheet. It has been reported in the previous theoretical studies[21] that vdW interaction is the predominant source of attraction between nucleobases and adsorbent. Therefore, it is important to include the vdW interactions in DFT calculations to accurately determine the adsorption energies. Thus, in the present work, we have used dispersion correction of Grimme's D3-type for DFT calculations (DFT-D3)[53] (for more detail about DFT-D3, see the SI) to study the interactions of nucleobases with BCN sheet.

The adsorption energy (E_{ad}) of nucleobases on BCN sheet was calculated using the following equation

$$E_{ad} = E_{BCN+nucleobase} - E_{BCN} - E_{nucleobase} \quad (4)$$

where $E_{BCN+nucleobase}$ is the total energy of the BCN with nucleobase, E_{BCN} represents the total energy of bare BCN, and $E_{nucleobase}$ denotes the energy of the nucleobase. All calculations were carried out using QUANTUM ESPRESSO package.[54]

ASSOCIATED CONTENT

Supporting Information

The Supporting Information is available free of charge on the ACS Publications website at DOI: 10.1021/acsomega.8b03454.

Converged parameters for cutoff energy and K-point mesh; HOMO and LUMO energy of nucleobases;

DOI: 10.1021/acsomega.8b03454
ACS Omega 2019, 4, 3732–3738

optimized structures of nucleobases and BCN sheet (PDF)

AUTHOR INFORMATION

Corresponding Author

*E-mail: jayantks@iitk.ac.in.

ORCID

Showkat Hassan Mir: 0000-0002-9291-4680
Vivek Kumar Yadav: 0000-0002-9142-4567
Jayant Kumar Singh: 0000-0001-8056-2115

Notes

The authors declare no competing financial interest.

ACKNOWLEDGMENTS

S.H.M. and V.K.Y. gratefully acknowledge the financial support from Department of Science and Technology (grant nos. SB/S3/CE/079/2015 and DST/TM/WTI/2K15/112(G)). The calculations were partly done at the High Performance Computing Facility at the Computer Center, IIT Kanpur.

REFERENCES

(1) Sowerby, S. J.; Cohn, C. A.; Heckl, W. M.; Holm, N. G. Differential adsorption of nucleic acid bases: Relevance to the origin of life. *Proc. Natl. Acad. Sci. U.S.A.* **2001**, *98*, 820−822.

(2) Mukhopadhyay, S.; Gowtham, S.; Scheicher, R. H.; Pandey, R.; Karna, S. P. Theoretical study of physisorption of nucleobases on boron nitride nanotubes: a new class of hybrid nano-biomaterials. *Nanotechnology* **2010**, *21*, No. 165703.

(3) Lu, C.; Liu, Y.; Ying, Y.; Liu, J. Comparison of mos2, ws2, and graphene oxide for dna adsorption and sensing. *Langmuir* **2017**, *33*, 630−637.

(4) Yang, K.; Feng, L.; Shi, X.; Liu, Z. Nano-graphene in biomedicine: theranostic applications. *Chem. Soc. Rev.* **2013**, *42*, 530−547.

(5) Jones, M. R.; Seeman, N. C.; Mirkin, C. A. Programmable materials and the nature of the dna bond. *Science* **2015**, *347*, No. 1260901.

(6) Tan, L. H.; Xing, H.; Lu, Y. Dna as a powerful tool for morphology control, spatial positioning, and dynamic assembly of nanoparticles. *Acc. Chem. Res.* **2014**, *47*, 1881−1890.

(7) Wang, H.; Yang, R.; Yang, L.; Tan, W. Nucleic acid conjugated nanomaterials for enhanced molecular recognition. *ACS Nano* **2009**, *3*, 2451−2460.

(8) Liu, J.; Cao, Z.; Lu, Y. Functional nucleic acid sensors. *Chem. Rev.* **2009**, *109*, 1948−1998.

(9) Song, S.; Qin, Y.; He, Y.; Huang, Q.; Fan, C.; Chen, H. Y. Functional nanoprobes for ultrasensitive detection of biomolecules. *Chem. Soc. Rev.* **2010**, *39*, 4234−4243.

(10) Novoselov, K. S.; Fal, V. I.; Colombo, L.; Gellert, P. R.; Schwab, M. G.; Kim, K. A roadmap for graphene. *Nature* **2012**, *490*, 192.

(11) Zhang, C. Y.; Yeh, H. C.; Kuroki, M. T.; Wang, T. H. Singlequantum-dot-based dna nanosensor. *Nat. Mater.* **2005**, *4*, 826.

(12) Lu, W.; Qin, X.; Luo, Y.; Chang, G.; Sun, X. CdS quantum dots as a fluorescent sensing platform for nucleic acid detection. *Microchim. Acta* **2011**, *175*, 355−359.

(13) Vovusha, H.; Sanyal, B. Adsorption of nucleobases on 2d transition-metal dichalcogenides and graphene sheet: a first principles density functional theory study. *RSC Adv.* **2015**, *5*, 67427−67434.

(14) Liu, B.; Salgado, S.; Maheshwari, V.; Liu, J. DNA adsorbed on graphene and graphene oxide: Fundamental interactions, desorption and applications. *Curr. Opin. Colloid Interface Sci.* **2016**, *26*, 41−49.

(15) Park, J. S.; Goo, N. I.; Kim, D. E. Mechanism of dna adsorption and desorption on graphene oxide. *Langmuir* **2014**, *30*, 12587−12595.

(16) Lu, C.; Huang, P. J.; Liu, B.; Ying, Y.; Liu, J. Comparison of graphene oxide and reduced graphene oxide for dna adsorption and sensing. *Langmuir* **2016**, *32*, 10776−10783.

(17) Lee, J.; Yim, Y.; Kim, S.; Choi, M.; Choi, B.; Lee, Y.; Min, D. H. Indepth investigation of the interaction between dna and nano-sized graphene oxide. *Carbon* **2016**, *97*, 92−98.

(18) Yang, R.; Jin, J.; Chen, Y.; Shao, N.; Kang, H.; Xiao, Z.; Tang, Z.; Wu, Y.; Zhu, Z.; Tan, W. Carbon nanotube-quenched fluorescent oligonucleotides: probes that fluoresce upon hybridization. *J. Am. Chem. Soc.* **2008**, *130*, 8351−8358.

(19) Xu, W.; Xue, X.; Li, T.; Zeng, H.; Liu, X. Ultrasensitive and selective colorimetric dna detection by nicking endonuclease assisted nanoparticle amplification. *Angew. Chem., Int. Ed.* **2009**, *48*, 6849−6852.

(20) Leenaerts, O.; Partoens, B.; Peeters, F. M. Adsorption of H2O, NH3, CO, NO2, and NO on graphene: A first-principles study. *Phys. Rev. B* **2008**, *77*, No. 125416.

(21) Gowtham, S.; Scheicher, R. H.; Ahuja, R.; Pandey, R.; Karna, S. P. Physisorption of nucleobases on graphene: Density-functional calculations. *Phys. Rev. B* **2007**, *76*, No. 033401.

(22) Ding, N.; Chen, X.; Wu, C. M. L.; Li, H. Adsorption of nucleobase pairs on hexagonal boron nitride sheet: hydrogen bonding versus stacking. *Phys. Chem. Chem. Phys.* **2013**, *15*, 10767−10776.

(23) Seyed-Talebi, S. M.; Neek-Amal, M. The different adsorption mechanism of methane molecule onto a boron nitride and a graphene flakes. *J. Appl. Phys.* **2014**, *116*, No. 153507.

(24) Zhou, M.; Lu, Y. H.; Cai, Y. Q.; Zhang, C.; Feng, Y. P. Adsorption of gas molecules on transition metal embedded graphene: a search for high-performance graphene-based catalysts and gas sensors. *Nanotechnology* **2011**, *22*, No. 385502.

(25) Antony, J.; Grimme, S. Structures and interaction energies of stacked graphene-nucleobase complexes. *Phys. Chem. Chem. Phys.* **2008**, *10*, 2722−2729.

(26) Le, D.; Kara, A.; Schrøder, E.; Hyldgaard, P.; Rahman, T. S. Physisorption of nucleobases on graphene: a comparative van der waals study. *J. Phys.: Condens. Matter* **2012**, *24*, No. 424210.

(27) Lin, Q.; Zou, X.; Zhou, G.; Liu, R.; Wu, J.; Li, J.; Duan, J. Adsorption of dna/rna nucleobases on hexagonal boron nitride sheet: an ab initio study. *Phys. Chem. Chem. Phys.* **2011**, *13*, 12225−12230.

(28) Han, W. Q.; Wu, L.; Zhu, Y.; Watanabe, K.; Taniguchi, T. Structure of chemically derived mono-and few-atomic-layer boron nitride sheets. *Appl. Phys. Lett.* **2008**, *93*, No. 223103.

(29) Pacilé, D.; Meyer, J. C.; Girit, C. O.; Zettl, A. The two-dimensional phase of boron nitride: Few-atomic-layer sheets and suspended membranes. *Appl. Phys. Lett.* **2008**, *92*, No. 133107.

(30) Novoselov, K. S.; Geim, A. K.; Morozov, S. V.; Jiang, D. A.; Zhang, Y.; Dubonos, S. V.; Grigorieva, I. V.; Firsov, A. A. Electric field effect in atomically thin carbon films. *Science* **2004**, *306*, 666−669.

(31) Watanabe, K.; Taniguchi, T.; Kanda, H. Direct-bandgap properties and evidence for ultraviolet lasing of hexagonal boron nitride single crystal. *Nat. Mater.* **2004**, *3*, 404.

(32) Hod, O. Graphite and hexagonal boron-nitride have the same interlayer distance. Why? *J. Chem. Theory Comput.* **2012**, *8*, 1360−1369.

(33) Barua, S.; Dutta, H. S.; Gogoi, S.; Devi, R.; Khan, R. Nanostructured MoS2-Based Advanced Biosensors: *A Review*. *ACS Appl. Nano Mater.* **2018**, *1*, 2−25.

(34) Jin, K.; Xie, L.; Tian, Y.; Liu, D. Au-modified monolayer MoS2 sensor for DNA detection. *J. Phys. Chem. C* **2016**, *120*, 11204−11209.

(35) Loan, P. T. K.; Zhang, W.; Lin, C. T.; Wei, K. H.; Li, L. J.; Chen, C. H. Graphene/MoS2 heterostructures for ultrasensitive detection of DNA hybridisation. *Adv. Mater.* **2014**, *26*, 4838−4844.

(36) Huang, Y.; Shi, Y.; Yang, H. Y.; Ai, Y. A novel single-layered MoS2 nanosheet based microfluidic biosensor for ultrasensitive detection of DNA. *Nanoscale* **2015**, *7*, 2245−2249.

(37) Watanabe, M. O.; Itoh, S.; Mizushima, K.; Sasaki, T. Electrical properties of BC2N thin films prepared by chemical vapor deposition. *J. Appl. Phys.* **1995**, *78*, 2880−2882.

DOI: 10.1021/acsomega.8b03454
ACS Omega 2019, 4, 3732−3738

(38) Xu, B.; Lu, Y. H.; Feng, Y. P.; Lin, J. Y. Density functional theory study of BN-doped graphene superlattice: Role of geometrical shape and size. *J. Appl. Phys.* **2010**, *108*, No. 073711.
(39) Ci, L.; Song, L.; Jin, C.; Jariwala, D.; Wu, D.; Li, Y.; Srivastava, A.; Wang, Z. F.; Storr, K.; Balicas, L.; Liu, F.; Ajayan, P. M. Atomic layers of hybridized boron nitride and graphene domains. *Nat. Mater.* **2010**, *9*, 430.
(40) Ba, K.; Jiang, W.; Cheng, J.; Bao, J.; Xuan, N.; Sun, Y.; Liu, B.; Xie, A.; Wu, S.; Sun, Z. Chemical and bandgap engineering in monolayer hexagonal boron nitride. *Sci. Rep.* **2017**, *7*, No. 45584.
(41) Manna, A. K.; Pati, S. K. Tunable Electronic and Magnetic Properties in B_x C_y N_z Nanohybrids: Effect of Domain Segregation. *J. Phys. Chem. C* **2011**, *115*, 10842−10850.
(42) Azevedo, S. Energetic stability of B−C−N monolayer. *Phys. Lett. A* **2006**, *351*, 109−112.
(43) Chhetri, M.; Maitra, S.; Chakraborty, H.; Waghmare, U. V.; Rao, C. N. R. Superior performance of borocarbonitrides, B_x C_y N_z, as stable, low-cost metal-free electrocatalysts for the hydrogen evolution reaction. *Energy Environ. Sci.* **2016**, *9*, 95−101.
(44) Preuss, M.; Schmidt, W. G.; Bechstedt, F. Coulombic amino group-metal bonding: Adsorption of adenine on Cu (110). *Phys. Rev. Lett.* **2005**, *94*, No. 236102.
(45) Özçelik, V. O.; Ciraci, S. Size dependence in the stabilities and electronic properties of α-graphyne and its boron nitride analogue. *J. Phys. Chem. C* **2013**, *117*, 2175−2182.
(46) Gürel, H. H.; Salmankurt, B. Binding mechanisms of DNA/RNA nucleobases adsorbed on graphene under charging: first-principles van der Waals study. *Mater. Res. Express* **2017**, *4*, No. 065401.
(47) Dabhi, S. D.; Roondhe, B.; Jha, P. K. Nucleobases-decorated boron nitride nanoribbons for electrochemical biosensing: a dispersion-corrected DFT study. *Phys. Chem. Chem. Phys.* **2018**, *20*, 8943−8950.
(48) Varghese, N.; Mogera, U.; Govindaraj, A.; Das, A.; Maiti, P. K.; Sood, A. K.; Rao, C. N. R. Binding of DNA nucleobases and nucleosides with graphene. *ChemPhysChem* **2009**, *10*, 206−210.
(49) Gossenberger, F.; Roman, T.; Forster-Tonigold, K.; Groß, A. Change of the work function of platinum electrodes induced by halide adsorption. *Beilstein J. Nanotechnol.* **2014**, *5*, 152.
(50) Perdew, J. P.; Burke, K.; Ernzerhof, M. Generalized gradient approximation made simple. *Phys. Rev. Lett.* **1996**, *77*, No. 3865.
(51) Rappe, A. M.; Rabe, K. M.; Kaxiras, E.; Joannopoulos, J. D. Optimized pseudopotentials. *Phys. Rev. B* **1990**, *41*, No. 1227.
(52) Monkhorst, H. J.; Pack, J. D. Special points for Brillouin-zone integrations. *Phys. Rev. B* **1976**, *13*, No. 5188.
(53) Grimme, S.; Antony, J.; Ehrlich, S.; Krieg, H. A consistent and accurate ab initio parametrization of density functional dispersion correction (DFT-D) for the 94 elements H-Pu. *J. Chem. Phys.* **2010**, *132*, No. 154104.
(54) Giannozzi, P.; Baroni, S.; Bonini, N.; Calandra, M.; Car, R.; Cavazzoni, C.; Dal Corso, A.; et al. QUANTUM ESPRESSO: a modular and open-source software project for quantum simulations of materials. *J. Phys.: Condens. Matter* **2009**, *21*, No. 395502.

DOI: 10.1021/acsomega.8b03454
ACS Omega 2019, 4, 3732−3738